Materials Letters 138 (2015) 255–258

Contents lists available at ScienceDirect

Materials Letters

journal homepage: www.elsevier.com/locate/matlet

# Transformations of Cu(in) supersaturated solid solutions under high-pressure torsion

B.B. Straumal [a,b,c,d,*], A.R. Kilmametov [b,e], A.A. Mazilkin [a,b], L. Kurmanaeva [b,f], Y. Ivanisenko [b], A. Korneva [g], P. Zięba [g], B. Baretzky [b]

[a] Institute of Solid State Physics, Russian Academy of Sciences, 142432, Chernogolovka, Russia
[b] Karlsruher Institut für Technologie, Institut für Nanotechnologie, 76344 Eggenstein-Leopoldshafen, Germany
[c] Moscow Institute of Physics and Technology (State University), Institutskii per. 9, 141700 Dolgoprudny, Russia
[d] National University of Science and Technology «MISIS», Leninskii prosp. 4, 119049 Moscow, Russia
[e] Institute of Physics of Advanced Materials, Ufa State Aviation Technical University, K. Marx St. 12, 450000 Ufa, Russia
[f] Department of Chemical Engineering & Materials Science, University of California, One Shields Avenue, Davis, CA 95616, USA
[g] Institute of Metallurgy and Materials Science, Polish Academy of Sciences, Reymonta St. 25, 30-059 Cracow, Poland

ARTICLE INFO

*Article history:*
Received 6 July 2014
Accepted 2 October 2014
Available online 14 October 2014

*Keywords:*
High-pressure torsion
Solid solution
Cu–In alloys
Phase transitions

ABSTRACT

High-pressure torsion of six homogenized Cu–In alloys (2.3 to 13.5 at. % In) with negative mixing enthalpy has been studied. The torsion torque reached a steady-state after 1–2 anvil rotations. Differently to the alloys with positive mixing enthalpy, the Cu(In) solid solution did not decompose. Moreover, the precipitates of δ-phase in the Cu–13.5 at. % In alloy partially dissolved and additionally enriched the Cu(In) solid solution.



## 1. Introduction

It has been well established that irradiation [1] and processes called "mechanical alloying" (MA) like ball milling [2–5] and severe plastic deformation (SPD) [6–8] can lead to the phase transformations. However, the mechanisms of such mechanically driven phase transitions are poorly understood up to now. Usually MA procedures have been applied to elemental powders blends, or to more or less equilibrium "matrix-precipitate" systems and they produced metastable solid solutions [2–5,9], amorphous [10] and quasi-crystalline [11] phases. Recently an opposite effect was explored when SPD was applied for metastable supersaturated solid solutions [12–15]. The supersaturated solid solutions in systems Al–Zn, Co–Cu, Cu–Ni and Cu–Ag decomposed after high-pressure torsion (HPT) straining. These systems possess a positive mixing enthalpy (Table 1) and do not contain any intermetallic compounds [16–24]. However, no systematic research was performed on SPD of supersaturated solid solutions of elements with negative mixing enthalpy and intermetallics. We have chosen the Cu–In system, which possesses negative mixing enthalpy (Table 1) and belongs to the broad class of Cu-alloys containing well-known Hume-Rothery intermetallic compounds. The conventional decomposition processes (like continuous and discontinuous precipitation, or spinodal decomposition) were thoroughly studied in Cu–In alloys in the past [25–29].

## 2. Experimental

Six Cu–In alloys with 2.3, 4, 5.8, 7, 9.5 and 13.5 at. % In have been prepared from high purity components (5 N Cu and In) by induction melting in vacuum in the form of cylindrical ingots. For HPT processing the 10 mm diameter and 0.6 mm thick discs were cut from the as-cast ingots, then ground and chemically etched. In order to prevent oxidation during high temperature anneal, the samples were sealed in evacuated silica ampoules with a residual pressure of approximately $4 \times 10^{-4}$ Pa at room temperature. Samples were annealed at $560 \pm 1$ °C for 840 h and then quenched in water. The annealed samples were subjected to HPT at room temperature under a pressure of 6 GPa in a Bridgman anvil-type unit (five rotations of the anvil with the rate of 1 rpm) using a custom-built computer-controlled HPT device (W. Klement GmbH, Lang, Austria). The torsion torque measured during HPT increased during 1–2 anvil rotations and then remained unchanged (i.e. reached the steady state as in Refs. [12–15]). Samples for

* Corresponding author at: Postal address: Institute of Solid State Physics, Russian Academy of Sciences, Chernogolovka, Moscow district, 142432 Russia.
Tel.: +7 916 6768673; fax: +7 499 2382326.
*E-mail address:* straumal@issp.ac.ru (B.B. Straumal).

http://dx.doi.org/10.1016/j.matlet.2014.10.009
0167-577X/

**Table 1**
Mixing enthalpy in studied alloys.

| Alloy | Cu–Ni | Cu–Co | Cu–Ag | Al–Zn | Cu–In |
|---|---|---|---|---|---|
| Mixing enthalpy, kJ/mol and literature source | +11.5 [17] | +10 [18] | +13 [19,20] | +2.5[21–23] | −5 [24] |

microstructural and X-rays investigations were cut from the HPT-processed discs at a distance of 3 mm from the sample center. The prior inspection of the obtained material was carried out on a Philips XL30 scanning electron microscope (SEM) equipped with an Oxford Instruments LINK ISIS energy-dispersive X-ray spectrometer (EDS). The details of the phases' composition and structure were investigated using a TECNAI G2 FEG super TWIN (200 kV) transmission electron microscope (TEM) equipped with an EDAX EDX system. Identification of the electron diffraction patterns was performed by the Process Diffraction program [30]. X-ray diffractograms were obtained using Bragg–Brentano geometry in a powder diffractometer (Philips X'Pert) with Cu-Kα radiation. The volume averaged crystallite size and the microstrain were estimated from the XRD peak broadening using a modified Williamson–Hall method [31]. All reflections with Miller indices up to (4 2 0) were used for the grain size and microstrains estimates. Lattice parameter values were estimated using powder diffraction tool of "Fityk" software" [32].

## 3. Results and discussion

Thin vertical lines in the Cu–In phase diagram (Fig. 1a) show the indium concentration in the studied alloys. A thin horizontal line shows the annealing temperature of 560 ± 1 °C. XRD patterns for the alloys with 2.3, 4, 5.8, 7, and 9.5 at. % In show that after annealing they contained only supersaturated solid solution Cu (In). The Cu–13.5 at. % In alloy contained the Cu-based solid solution with 10.7 at. % In and about 20% of δ-phase. The δ-phase is one of the Hume-Rothery intermetallic phases. It contains 29–31 at. % In and has $B8_1$ crystalline structure of NiAs type [33]. Filled circles in Fig. 1a show the concentration in the Cu matrix after annealing as measured by EDS (SEM). The filled circle for the Cu–13.5 at. % In corresponds to the maximum indium solubility at 560 °C and is on the solvus line. SEM measurements show also that the Cu(In) grain size in all alloys was about 50–100 μm; the size of δ-precipitates was about few microns. TEM observations revealed thin and relaxed grain boundaries in Cu(In) and interphase boundaries Cu(In)/δ-phase (see for example the boundary between Cu (left) and δ-precipitate (right) in Fig. 2a). Filled circles in Fig. 1b show the Cu(In) lattice spacing in homogenized alloys.

After HPT the grain and particle size drastically decreased. The Williamson–Hall method permitted to obtain the crystallite size (the size of coherently scattering domains) and microstrain in Cu (In) grains after HPT (Fig. 1c) from the shape of XRD peaks. Crystallite size after HPT decreased with increasing indium content (from 50 nm in pure Cu to about 5 nm at 13.5 at. % In). The microstrain, conversely, increased with increasing indium concentration (from 0.05% in pure Cu to 0.54% at 13.5 at. % In). TEM micrographs (Fig. 2b,c) reveal that Cu(In) grains after HPT are separated from each other by the broad and less-defined boundaries. After HPT δ-precipitates become extremely fine, only the first XRD peak (very broad and weak) of δ-phase remains visible. The electron diffraction patterns also contain the very weak rings of δ-phase. The high level of internal elastic stresses and distortions makes it impossible to image δ-precipitates after HPT by TEM, even in the dark-field micrographs (Fig. 2d, e). The open

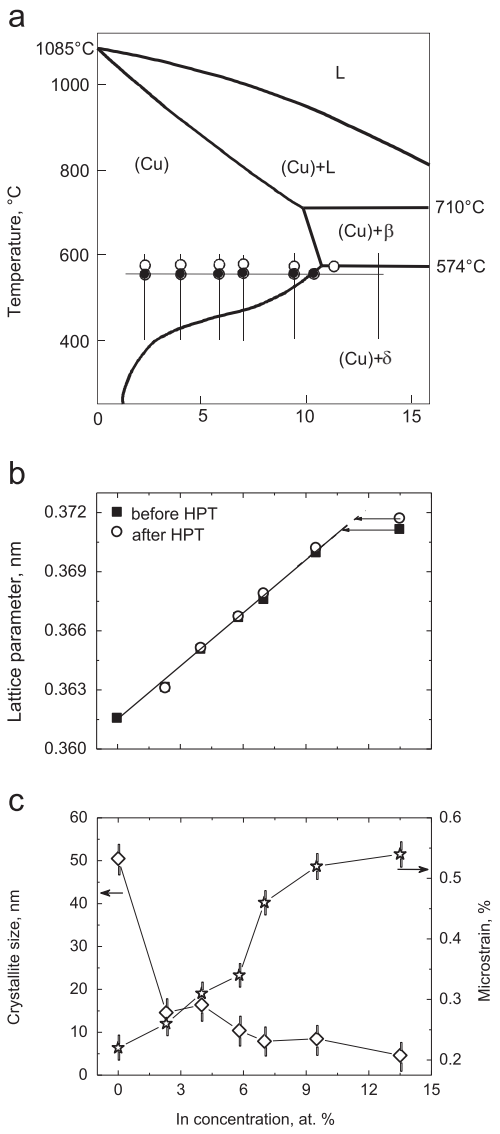


**Fig. 1.** (a) The Cu-rich part of the Cu–In phase diagram [16]. Thin vertical lines show the In concentration in the studied alloys. Thin horizontal line shows the annealing temperature. Filled circles show the concentration in the Cu-matrix after annealing and open circles show the concentration in the Cu-matrix after HPT. (b) Dependence of lattice spacing on the In concentration before (filled squares) and after HPT (open circles). The straight solid line between 0 and 11 at. % In is drawn through the experimental data for the lattice spacing in Cu(In) solid solutions obtained previously in the literature [34–37]. It continues above the maximal solubility as a broken line. The experimental points from the literature were omitted in order not to overload the figure. The arrows for the Cu–13.5 at. % In alloy show the composition in the Cu(In) matrix before and after HPT. Experimental error is less than symbol size. (c) Crystallite size or size of coherently scattering domains (diamonds) and microstrain (stars) obtained using Williamson–Hall method. Lines are the guides for the eye.

circles in Fig. 1a show the lattice spacing of the Cu(In) solid solution after HPT.

We have chosen six indium concentrations for our investigations. We expected, similar to the studied Cu–Ni alloys, that the supersaturated Cu(In) solid solutions would behave differently at

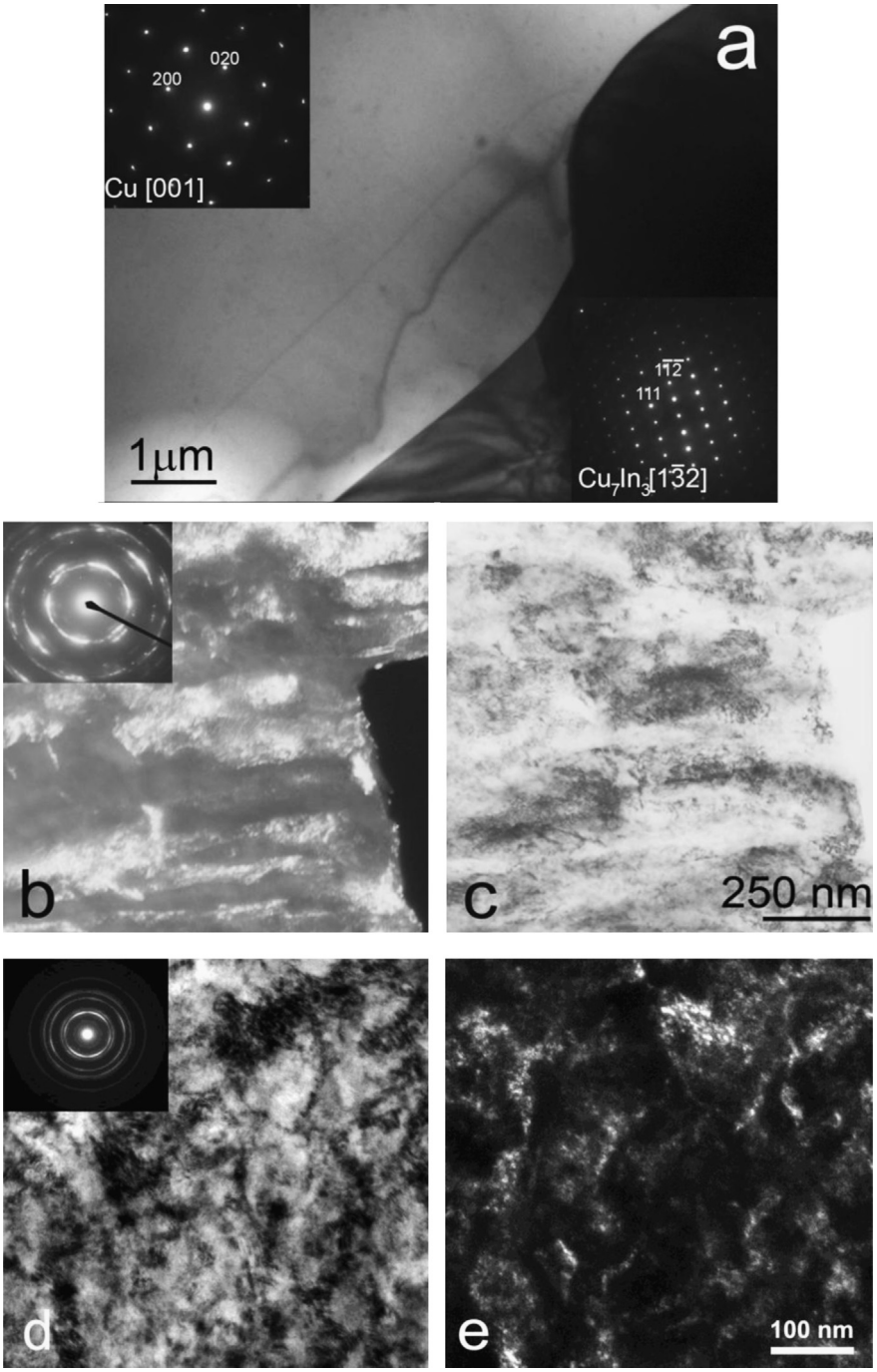


**Fig. 2.** TEM micrographs of Cu–13.5 at. % In (a, d, e) and Cu–9.5 at. % In (b, c) alloys after annealing at 560 °C for 840 h before (a) and after HPT (b to e). Insets show the respective electron diffraction patterns. (a) Cu grain (left) and δ-phase (right). (b, d) Bright field. (c, e) Dark field.

various In concentrations. Surprisingly, the result was rather unexpected. In the first five alloys the lattice spacing of the (Cu) solid solution did not change at all after HPT compared with the initial ones (e.g. open and filled circles in Fig. 1b). The straight solid line between 0 and 11 at. % In is drawn through the experimental data for the lattice spacing in Cu(In) solid solutions obtained previously [34–37]. The experimental points from the quoted references were omitted in order not to overload the figure. The lattice spacing in Cu(In) solid solutions follows the linear Vegard's law very good. Our experimental points for the five alloys before and after HPT correspond well with this solid line, lattice spacing linearly increases with increasing indium content. The arrows for the Cu–13.5 at. % In alloy show the composition in the Cu(In) matrix before and after HPT on the Vegard's law line.

In other words, the supersaturated Cu(In) solid solution did not decompose after HPT. This behavior is similar to the Cu-based solid solutions with low Ni content of 9 and 26 wt. % [15]. The supersaturated Cu(In) solid solution in the Cu–13.5 at. % In alloy also did not decompose. Moreover, the lattice spacing increased, pointing toward a corresponding increase of In content in the Cu matrix from 10.7 at. % before HPT to 11.4 at. % after (shown by the arrow in Fig. 1b and by the open circle in the phase diagram, Fig. 1a). It means that the precipitates of δ-phase in the Cu–13.5 at. % In alloy partially dissolved and thus enriched the Cu(In) solid

solution. 11 at. % is the maximal amount of indium which can be dissolved in copper at eutectoid temperature of 574 °C [16]. The Cu matrix in the Cu–13.5 at. % In alloy contained after HPT even slightly more indium, than would be contained after the annealing at 574 °C. Therefore, the open points in Fig. 1a are placed at 574 °C being the temperature of maximal In solubility in solid Ci (In) phase.

The grain size estimated from TEM dark field images in samples with lower indium content (Fig. 2b, c) is about 2–4 times larger than the crystallite size measured by XRD (Fig. 1c). It is because the Williamson–Hall method delivers the size of coherent scattering regions, which corresponds rather to subgrain than to grain size. We observed previously in the alloys with positive mixing enthalpy that the GBs after HPT are thin and well-defined, and the grain size in Cu-rich matrix was about 150–400 nm [12–15]. In the Cu–In alloys with negative mixing enthalpy the grain size is much smaller. Moreover, an increase of indium content led to a further drastic decrease of the grain size (like for example in alloys exhibiting solution hardening after ball milling [4]). Note that the grain boundaries are broad and less-defined. Such grain boundaries are often called nonequilibrium [38]. It looks like indium prevented the dynamic recrystallization of Cu matrix during HPT. At highest indium content the crystallite size and visible GB width become almost equal (Fig. 2d,e).

HPT of the Cu–13.5 at. % In alloy leads to the partial dissolution of δ-phase precipitates. We can estimate the equivalent diffusion coefficient $D_{HPT}$ for the results of this HPT-driven mass transfer from the simple equation $L=(D_{HPT}\,t)^{0.5}$, where $t=300$ s (being the HPT duration) and $L$ is the distance of the mass transfer. The initial rarely positioned few-micrometer large precipitates were substituted by the fine particles of nanometer size. The shortest possible distance for this HPT-driven mass transfer is comparable with a matrix grain size $L=20$ nm. Other estimations would give even larger values of $L$. Thus, $D_{HPT}=10^{-18}$ m/s$^{-2}$. The extrapolation of $D$ for Cu self-diffusion and In bulk diffusion in Cu to 300 K (temperature of HPT treatment) gives $D=10^{-35}$ m$^2$/s [39] and $D=10^{-39}$ m/s$^{-2}$ [40], respectively. Similar extrapolation of In GB diffusion coefficient gives $D_{GB}=10^{-28}$ m/s$^{-2}$ [26]. In spite of the fact that high pressure slows down both bulk and GB diffusion [41,42], the $D_{HPT}$ is 10 to 21 orders of magnitude higher than these extrapolated values. It means that, like in previously studied systems, HPT strongly accelerates mass transfer.

Most likely the difference in the behavior of Cu–In alloys in comparison with the previously studied Al–Zn, Co–Cu, Cu–Ni and Cu–Ag alloys can be due to the sign of the mixing enthalpy. The positive mixing enthalpy in these (Table 1) promotes the clustering of impurity atoms. Therefore, in case of positive mixing enthalpy the impurity atoms would tend to form a kind of zone or precipitate in the supersaturated solid solution, The HPT treatment would speed up this decomposition by delivering nonequilibrium vacancies.

The negative mixing enthalpy in the Cu–In alloys thermodynamically prevents the alloy decomposition during HPT. Remaining in solid solution, In atoms promote grain refinement down to a nanoscale range (Figs. 1c, 2e). It has been frequently argued that the large volume fraction of grain boundaries present in nanocrystalline state enhances the solid solubility in these materials [3,4]. That is why partial dissolution of the δ-phase precipitates in Cu – 13.5 at. % In alloy after HPT was possible, leading to the increased concentration of In in the Cu matrix as compared with that after the annealing at 574 °C.

## 4. Conclusions

The Cu–In supersaturated solid solution during HPT behaves differently as compared to Al–Zn, Co–Cu and Cu–Ni systems with positive mixing enthalpy and without intermetallic phases. It does not decompose during HPT. Furthermore, in the Cu–13.5 at. % In alloy, the δ-phase particles partially dissolve in the Cu-matrix, leading to its additional enrichment with indium. As a result, the concentration of indium in the Cu-matrix becomes at least as high as a sample annealed at 574 °C.

## Acknowledgments

The work was partially supported by the Russian Foundation for Basic Research (grants 14-08-00972 and 13-08-90422), EraNet.Rus programme (grant STProjects-219) and Karlsruhe Nano Micro Facility. TEM and SEM studies were supported by Polish National Science Centre (grant DEC-2011/01/M/ST8/07822).

## References

[1] Martin G, Bellon P. Solid State Phys 1997;50:189–331.
[2] Schwarz RB, Koch CC. Appl Phys Lett 1986;49:146–8.
[3] Fecht H-J. Formation of nanostructures by mechnical attrition. In: Edestein AS, Cammarata RC, editors. Nanomaterials: synthesis, properties, and application, Bristol: Institute of Physics. J.W. Arrowsmith LTD; 1996. p. 89–102.
[4] Suryanarayana C, Froes FH. J Mater Res 1990;5:1880–6.
[5] Pabi SK, Joardar J, Murty BS. Proc Ind Nac Sci Ac A 2001;67:1–30.
[6] Sauvage X, Chbihi A, Quelennec X. J Phys Conf Ser 2010;240:012003.
[7] Straumal BB, Sauvage X, Baretzky B, et al. Scripta Mater 2014;70:59–62.
[8] Straumal B, Korneva A, Zięba P. Arch Civil Mech Eng 2014;14:242–9.
[9] Pouryazdan M, Schwen D, Wang D, et al. Phys Rev B 2012;86:144302.
[10] Schwarz RB, Petrich RR, Saw CK. J Non-Cryst Sol 1985;76:281–302.
[11] Eckert J, Schultz L, Urban K. Appl Phys Lett 1989;55:117–9.
[12] Straumal B, Valiev R, Kogtenkova O, et al. Acta Mater 2008;55:6123–31.
[13] Straumal BB, Mazilkin AA, Baretzky B, et al. Mater Trans 2012;53:63–75.
[14] Straumal BB, Kilmametov AR, Kucheev YuO, et al. Mater Lett 2014;118:111–4.
[15] Straumal BB, Protasova SG, Mazilkin AA, et al. J Mater Sci 2012;47:360–7.
[16] Binary alloy phase diagrams. In: Massalski TB, editor. Materials Park, OH: ASM International; 1990.
[17] Yang HW, Tao DP, Zhou ZH. Acta Metall Sin Engl Lett 2008;21:336–40.
[18] Gente C, Oehring M, Bormann R. Phys Rev B 1993;48:13244.
[19] Fitzner K, Guo Q, Wang J, et al. J Alloys Comp 1999;291:190–200.
[20] Mazzone G, Rosato V, Pintore M, et al. Phys Rev B 1997;55:837–42.
[21] Hultgren R, Desai PD, Hawkins DT, et al. Selected values of the thermodynamic properties binary alloys. Metals Park, OH: American Society of Metals; 1973.
[22] Iqbal M, Shaikh MA, Akhter JI, et al. J Mater Sci 2004;39:4255–62.
[23] an Mey S. Z Metallkd 1993;84:451–5.
[24] Knott S, Mikula A. Int J Mater Res 2006;97:1098–101.
[25] Predel B, Gust W. Mater Sci Eng 1975;17:41–50.
[26] Gust W, Predel B, Roll U. Acta Metall 1980;28:1395–405.
[27] Manna I, Pabi K, Gust W. J Mater Sci 1999;34:1815–21.
[28] López GA, Zięba P, Gust W, et al. Mater Sci Technol 2003;19:1539–45.
[29] López GA, Zięba P, Gust W, et al. Microchim Acta 2004;145:101–5.
[30] Lábár JL. Microsc Microan 2008;14:287–95.
[31] Markmann J, Yamakov V, Weissmueller J. Scripta Mater 2008;59:15–8.
[32] Wojdyr M. J Appl Cryst 2010;43:1126–8.
[33] Hellner E, Laves F. Z. Naturforsch A 1947;2:177–83.
[34] Weibke F, Eggers H. Zt Anorgan Allgem Chem 1934;220:273–92.
[35] Owen EA, EAO Roberts. J Inst Met 1953;81:479–80.
[36] Jones RO, Owen EA. J Inst Met 1954;83:445–8.
[37] Stirling PH, Raynor GV. J Inst Met 1956;84:519–20.
[38] Sauvage X, Wilde G, Divinski SV, et al. Mater Sci Eng A 2012;540:1–12.
[39] Fujikawa S, Hirano KI. Bulk self diffusion in copper. In: Takamura JI, Doyama M, Kiritani M, editors. Proc. of yamada Vth Conf. on point defects, defect interactions in metals. Tokyo: Univ. of Tokyo Press; 1982. p. 554–8.
[40] Gorbachev VA, Klotsman SM, Rabovskiy YaA, et al. Phys Met Metallogr 1972;34(4):202–6.
[41] Straumal BB, Klinger LM, Shvindlerman LS. Scripta metal 1983;17:275–9.
[42] Molodov DA, Straumal BB, Shvindlerman LS. Scripta metal 1984;18:207–11.